ACS MATERIALS LETTERS

www.acsmaterialsletters.org

LETTER

Graphoepitaxy-Directed Assembly of Organic Semiconductor Single Crystals into Trellis Structures

Kai Zong, Kaustubh M. Asawa, Abigail Circelli, Nicholas Sparta, Chang-Hwan Choi, and Stephanie S. Lee*

Cite This: *ACS Materials Lett.* 2020, 2, 721–726

Read Online

ACCESS | Metrics & More | Article Recommendations | Supporting Information

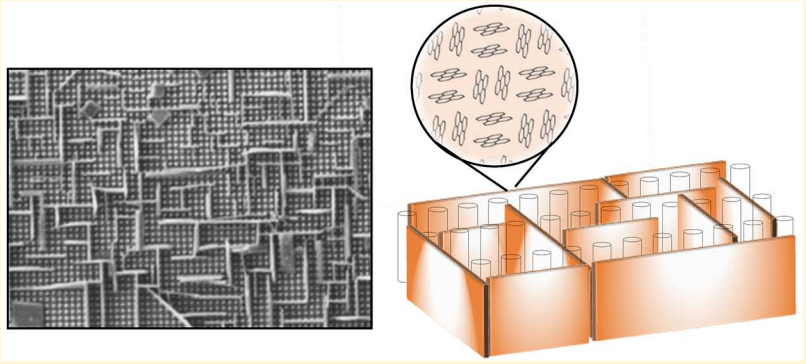

ABSTRACT: **In the field of organic electronics, organizing crystals into structures that promote efficient optoelectronic processes during rapid solution processing remains an outstanding challenge. Here, nanopillar grids are employed to direct the crystallization of organic semiconductor perylene during continuous solution-phase dip coating. These platelike crystals are found to orient in two distinct out-of-plane orientations with the large-area faces either parallel or perpendicular to the substrate surface. Perpendicular crystals are further found to adopt the underlying grid ordering, with crystals preferentially growing between the rows and columns of nanopillars to form structures resembling trellises. This observation of graphoepitaxy is a consequence of registry between the periodicity of the nanopillar grid and the growth habit of perylene, resulting in three-dimensional structures with ordering spanning the molecular to micrometer length scale. The ability to direct crystals into hierarchical structures with optimized orientations, surface areas, and sizes will have broad implications across materials disciplines.**

Organic semiconductor single crystals are considered to be the "gold standard" in the field of organic electronics, because of their near-perfect molecular ordering.[1,2] However, processing single crystals into complex architectures that are required for many optoelectronic devices remains an outstanding critical challenge, especially in the realm of solution processing of these materials to decrease manufacturing costs.[3] In particular, organic semiconductor crystals transport charge anisotropically along different crystallographic directions, with the fastest charge transport occurring along the direction of maximum π-orbital overlap.[4,5] For solution-processable organic semiconductors, interactions between solubilizing sides groups and the underlying substrate dominate out-of-plane crystal orientations in deposited films.[6] While selective nucleation of organic semiconductor single crystals onto patterned self-assembled monolayers can be used to form organized single-crystal arrays,[7] doing so in a manner that also orients the π-stack direction with the charge transport direction in sandwich-electrode device architectures to maximize device performance remains exceedingly difficult.

Graphoepitaxy, which was originally developed to grow oriented silicon films,[8,9] presents a promising strategy to guide the crystallization of soft matter systems into predetermined patterns. This method does not require lattice registry between

Received: April 15, 2020
Accepted: May 27, 2020
Published: May 27, 2020

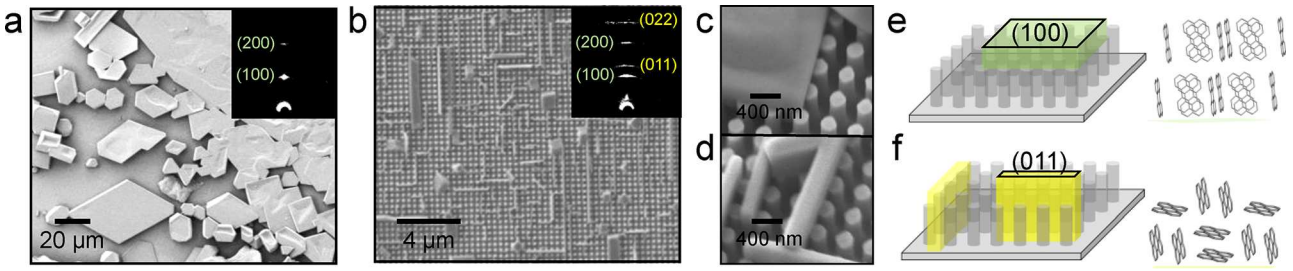

Figure 1. Scanning electron microscopy (SEM) micrographs and corresponding two-dimensional (2D) X-ray diffraction (XRD) patterns of perylene crystals deposited via dip coating on (a) a flat SiO_2 substrate and (b) a Si substrate patterned with Si nanopillars ($d_{spacing}$ = 370 nm). Major reflections observed along q_{xy} = 0 $Å^{-1}$ are labeled in the XRD patterns. (c and d) SEM micrographs of (100)-oriented crystals (panel (c)) and (011)-oriented crystals (panel (d)), collected at a tilt angle of 30°. (e and f) Illustrations of (100)-oriented crystals (panel (e)) and (011)-oriented crystals (panel (f)) within nanopillar grids (crystallographic faces corresponding to these planes are highlighted with a black line). Views of the molecular packing perpendicular to the (100) and (011) planes are also provided.

the crystals and the underlying substrate at the molecular level, but instead uses the geometry and/or periodicity of surface structures to impose long-range ordering on materials, including small molecules[10−12] and block copolymers.[13−15] The earliest reports of graphoepitaxy in molecular systems found that the ledges of freshly cleaved organic crystals could be used to direct the oriented crystallization of other organic compounds, as a result of registry between the angle of the ledge and the angle between specific crystal planes.[10,11] While crystallographic angles are dependent on the structure of compounds, they are not *unique* to specific molecular systems. Unlike molecular epitaxy, graphoepitaxy in this manner thus does not require matching between atomic positions of the templating surface and the deposited layer. Following this same principle, nanopores with angled corners defined by nanoparticle imprint lithography were later used to crystallize aspirin in preferential orientations.[12] Graphoepitaxy exploiting periodic surface structures has also been extensively employed to impose long-range ordering in microphase-separated block copolymer films.[13−15] Hexagonal arrays of nanopillars, for example, were used to direct the assembly of polystyrene-*b*-polydimethylsiloxane block copolymers into spherical domains that organized in registry with the underlying nanopillar pattern.[15]

To the best of our knowledge, graphoepitaxy using periodic surface structures to direct the long-range ordering of solution-processed organic semiconductor crystals has not yet been demonstrated. While several examples using nanogrooves in underlying substrates to direct crystallization have been reported,[16−18] oriented crystallization was induced by confinement of the crystals within the grooves, not the periodicity of the grooves themselves. Similarly, we recently demonstrated the use of nanoporous anodized aluminum oxide scaffolds to direct the growth of needle-like triisopropylsilylethynyl pyranthrene (TIPS-PY) crystals into vertical crystal arrays.[6] In that previous work, we discovered that the presence of nanoconfining scaffolds could orient crystal nuclei at the air/solution/scaffold interface to form large-surface area vertical crystal arrays with out-of-plane orientations optimized for light absorption and emission. In these examples, nanoconfinement selects for preferred crystal orientations in which the fast crystallization direction aligns with the long axis of the confining well,[18,19] but does not result in long-range ordering of the crystals in the plane of the film.

Here, we explore the influence of the periodicity of underlying nanoconfining scaffolds on crystal orientation in three dimensions during continuous solution deposition to arrange organic semiconductor crystals into ordered three-dimensional (3D) arrays. Specifically, we employed scaffolds consisting of ordered nanopillar grids with diameters, heights, and spacings on the order of hundreds of nanometers in length to direct crystallization during the dip coating of model perylene crystals from solution in chloroform. Perylene, which is a widely studied organic semiconductor with limited solubility in organic solvents, can exist in two polymorphs, α and β, both of which adopt a herringbone packing motif.[20,21] In agreement with previous reports in the literature,[22−24] we observed perylene crystals deposited via dip coating from solution onto SiO_2 substrates to form flat plates. As displayed in Figure 1a, these plates lie parallel to the substrate. The 2D XRD pattern collected on this film revealed that perylene exists in the thermodynamically favored α-polymorph, with a single out-of-plane orientation in which the (100) plane lies parallel to the substrate surface (Figure 1a inset; refer to Figure S1 in the Supporting Information for one-dimensional (1D) line traces). In this orientation, the π-stack direction is parallel to the substrate surface, which is typical of solution-processed organic semiconductors deposited onto flat substrates.[25,26] This orientation is promoted through substrate−crystal interactions that favor low-surface-energy crystal planes to be in contact with the underlying substrate.

To examine the ability of ordered scaffolds to direct nucleation and crystallization, we next deposited perylene crystals via dip coating onto Si substrates patterned with nanopillars defined by holographic lithography.[27−31] Because chloroform wets hydrophilic Si and SiO_2 surfaces (Figure S2 in the Supporting Information) and the Wenzel wetting theory predicts that texturing of hydrophilic surfaces increases their hydrophilicity,[32] complete wetting of the solution within the nanopillar grid is expected. Figure 1b displays an SEM micrograph of perylene crystals deposited on a grid with nanopillar heights, diameters and center-to-center spacings of 470, 170, and 370 nm, respectively. Surprisingly, two populations of platelike crystals were observed. In one population, the large faces of the crystals are oriented parallel to the substrate surface (Figure 1c). In the second population of crystals, the thin edges of the platelike crystals were exposed at the film surface and the large faces of the crystals oriented perpendicular to the substrate surface (Figure 1d). The corresponding 2D XRD pattern displayed in the inset in Figure 1b confirms the existence of two distinct out-of-plane orientations of α-phase crystals, one with the (100) plane

https://dx.doi.org/10.1021/acsmaterialslett.0c00153
ACS Materials Lett. 2020, 2, 721−726

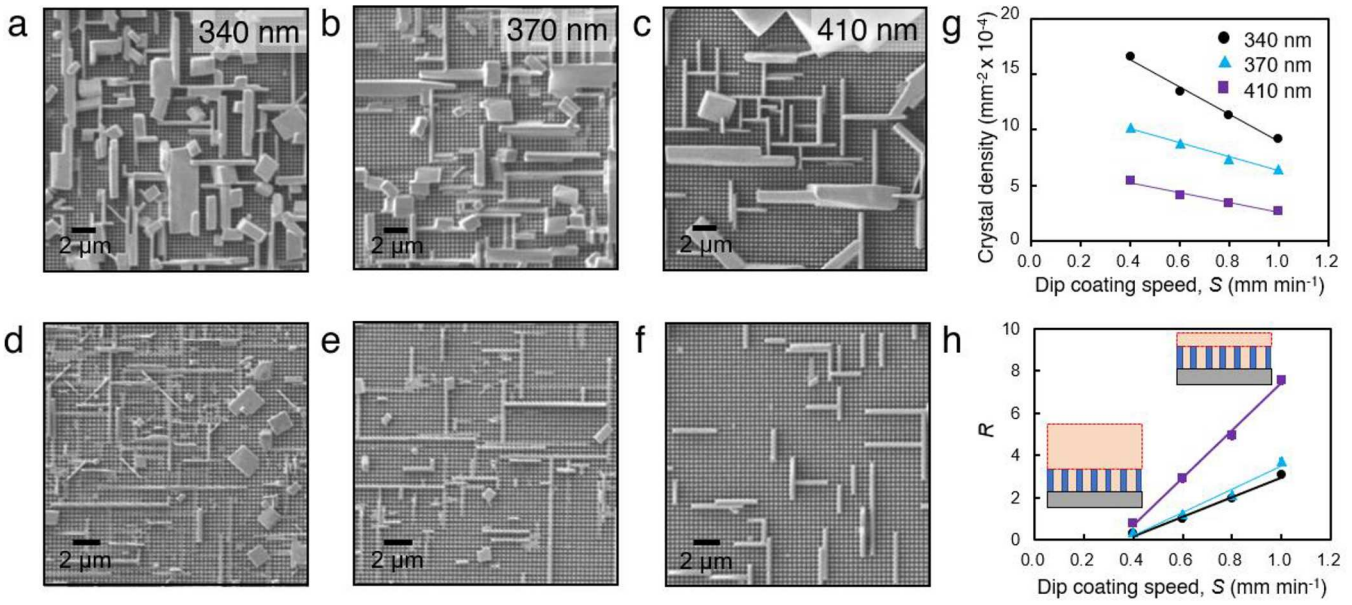

Figure 2. Top-view SEM images of perylene crystals dip-coated onto Si nanopillar grids at (a–c) S = 0.4 mm min^{-1} and (d–f) S = 1.0 mm min^{-1} for nanopillar spacings of 340, 370, and 410 nm, respectively. (g) Crystal density versus S for different nanopillar spacings. (h) Ratio of (011)- to (100)-oriented crystals (R), as a function of S for grids with different nanopillar spacings. Illustrations of the solution height, relative to the nanopillar grid at small and large dip-coating speeds, are also provided, with red dashed lines indicating the solution height above the nanopillar grids where (100)-oriented crystals are expected to nucleate. R was calculated for an average of 300 crystals per sample.

parallel to the substrate surface and the other with the (011) plane parallel to the substrate surface. Figures 1e and 1f display illustrations of the molecular ordering inside these two populations of crystals consistent with the SEM micrographs and XRD analysis. As observed in Figure 1f, the π-stack direction is aligned vertically from the substrate surface for (011)-oriented crystals. This orientation represents a critical finding in the field of solution-processed organic electronics. In sandwich-electrode device architectures, current is transported vertically through the organic active layer. To maximize current flow, for example, in solar cells and light-emitting diodes, the π-stack direction should therefore lie perpendicular to the substrate surface. For this class of materials, achieving this out-of-plane orientation remains a significant obstacle.

Intriguingly, (011)-oriented crystals generally adopted two specific in-plane orientations, as imposed by the nanopillar array. These crystals grow in the continuous empty spaces between rows or columns of nanopillars in approximately equal amounts, joining at 90° angles when two such crystals grow into each other to form interconnected trellises. For comparison, perylene crystals grown from solution onto aperiodic anodized aluminum oxide scaffolds with 1D cylindrical nanopores adopt a preferential out-of-plane orientation but random in-plane orientations (Figure S3 in the Supporting Information). In this case, we expect specific out-of-plane orientations to be induced via nanoconfinement, which is a phenomenon observed across materials classes, including small molecules, polymers, and inorganic compounds.[18,33,34] In these systems, 2D nanoconfinement is typically imposed by cylindrical nanopores of, for example, anodized aluminum oxide. Crystal nuclei oriented with their fast growth direction parallel to the unconfined direction of the cylindrical pore can reach the critical nucleus size more quickly than misoriented nuclei, resulting in a preferred orientation of crystals embedded within the nanopores.[33]

In contrast to perylene crystals grown from AAO scaffolds with aperiodic cylindrical nanopores, we do not expect nanoconfinement to play a significant role in guiding the crystal orientation of perylene crystals grown from solution onto nanopillar arrays. In this geometry, crystals are only partially confined in two dimensions. Furthermore, the spacings between nanopillars are one to two orders of magnitude larger than the expected critical nucleus size of organic small molecules.[35] Therefore, it is unlikely that the selection of preferred orientations occurs during crystal nucleation within the nanopillar grids.

Instead, we speculate that the ability of the nanopillar grid to direct the in-plane orientations of (011)-oriented crystals is a result of Ostwald ripening at the liquid/air/grid interface during solution dip coating. During this process, smaller, misoriented crystals within the grids dissolve, while crystals that have more space to grow, i.e., those oriented such that their fast growth direction is aligned with the unconfined empty spaces within the nanopillar grid, continue to enlarge (see Figure S4 in the Supporting Information). This size-dependent dissolution and growth process is driven by chemical potential differences between small and large crystals, with the former exhibiting higher chemical potential, because of larger surface area-to-volume ratios (see Figure S5 in the Supporting Information). The marked absence of small, misoriented crystals in the nanopillar grids is also evidence that Ostwald ripening is occurring during the dip-coating process. Through this process, graphoepitaxy-induced ordering of perylene crystals is therefore a consequence of registry between the nanopillar grid periodicity and the platelike growth habit of perylene crystals. Platelike anthracene crystals also adopt specific in-plane orientations imposed by the nanopillar grid (see Figure S6 in the Supporting Information). In contrast, when crystals that have a tendency to grow as needles (TIPS-PY, for example) are deposited on such nanopillar grids, we do not observe preferential in-plane

https://dx.doi.org/10.1021/acsmaterialslett.0c00153
ACS Materials Lett. 2020, 2, 721–726

crystal orientations with the grid pattern (Figure S7 in the Supporting Information).

Systematic characterization of the density and orientation of perylene crystals deposited on nanopillar grids, as a function of dip coating speed (S) and the nanopillar center-to-center spacing ($d_{spacing}$), was performed to understand the key parameters governing graphoepitaxy-induced crystal orientation. Figures 2a–c display top-view SEM images of perylene crystals dip-coated onto nanopillar grids at a rate of S = 0.4 mm min^{-1}, with $d_{spacing}$ = 340, 370, and 410 nm, respectively (refer to Table S1 in the Supporting Information for corresponding nanopillar heights and diameters). Consistent with our initial findings displayed in Figure 1, all samples exhibited both (011)- and (100)-oriented crystals, with (011)-oriented crystals aligning with the pattern imposed by the nanopillar grid. For smaller nanopillar spacings, (011)-oriented crystals that aligned diagonally through the grid structure were also occasionally observed. With an increase in nanopillar spacing, crystal densities decreased, average crystal sizes increased, and the proportion of (011)-oriented crystals increased. When S was increased to 1.0 mm min^{-1} (Figures 2d–f), the same trends were observed, with an overall decrease in the crystal densities and number of (100)-oriented crystals, compared to the samples dip-coated at 0.4 mm min^{-1}.

Figures 2g and 2h quantify the crystal densities per unit area and the ratio of (011)- to (100)-oriented crystals (R), respectively, as a function of the dip-coating speed and nanopillar spacing. Crystal densities were observed to decrease both with increasing dip-coating speed and nanopillar spacing. On the other hand, R was observed to increase both with increasing dip coating speed and nanopillar spacing. These trends can be understood through hydrodynamics in film formation. At relatively slow dip-coating speeds in the range of 0.4–1.0 mm min^{-1}, film deposition occurs in the evaporation regime in which the film thickness decreases as the speed increases, according to eq 1:[36]

$$h_f = \frac{C}{\rho L}\left(\frac{Q_{evap}}{S}\right) \quad (1)$$

where h_f is the film height, C the solute concentration, ρ the solute density, Q_{evap} the solvent evaporation rate, L the width of the film, and S the dip-coating speed. Of these variables, only S was varied in our experiments. The film height (h_f) decreases as S increases, resulting in a smaller amount of perylene deposited per unit area and thus lower crystal densities. The trend of decreasing crystal density with increasing nanopillar spacing is likely due to smaller friction to flow by the grids with larger spacings, resulting in a smaller amount of the liquid film left on the surface upon withdrawal.[37] The larger volume available for perylene crystallization to occur in larger nanopillar spacings may also facilitate Ostwald ripening, resulting in the formation of fewer, but larger, crystals.

The increase of R with S is also related to the film height. As h_f decreases with increasing S, so does the amount of fluid above the nanopillar grid. On the other hand, the amount of fluid within the nanopillar grid remains unchanged (Figure 2h, inset). Consistent with this observation, we speculate that (100)-oriented crystals nucleated on top of the grids, adopting the typical orientation of perylene crystals formed on unconfined surfaces. On the other hand, (011)-oriented crystals nucleated within the grids during dip coating. Because of the confinement imposed by the nanopillar grids, these crystals adopted an out-of-plane orientation that aligned their fast growth direction with the unconfined direction of the nanopillar grid. In contrast, perylene crystals deposited via drop casting onto nanopillar grids nucleated randomly on top of the grids, because of a large solution film height above the nanopillar grids (see Figure S8 in the Supporting Information).

Interestingly, R also varied significantly with the grid geometry. For the condition in which S = 1.0 mm min^{-1} and $d_{spacing}$ = 340 nm (Figure 2d), R was measured to be ~3.2 (Figure 2h). For comparison, R increased to ~7.5 (Figure 2h) when $d_{spacing}$ = 410 nm for the same dip-coating speed (Figure 2f). This trend can be understood by considering that the nanopillar grid itself occupies some finite volume. Figure 3a displays cross-sectional SEM micrographs of the nanopillar grids for the three different $d_{spacing}$ values. As observed from the images, both the spacing and nanopillar geometry varies among the three grids (also see Table S1 in the Supporting Information). For grids with $d_{spacing}$ = 340 nm, the nanopillars form cylindrical columns, whereas for larger spacings, the nanopillars form truncated cones.

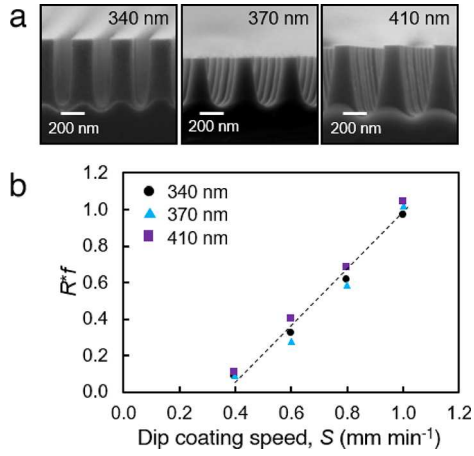

Figure 3. (a) Cross-sectional SEM images of nanopillar grids with center-to-center spacings of 340, 370, and 410 nm. (b) Plot of *Rf* versus *S*, where *f* is the fraction of volume occupied by the nanopillars, for the three different nanopillar spacings.

Considering that R is a dimensionless number, we sought to identify a dimensionless scaling factor that generalizes the dependence of R on S for different nanopillar geometries. Specifically, a second dimensionless number f was defined as the volume fraction occupied by the nanopillars. Accounting for the different nanopillar shapes, f was determined to be almost equal for $d_{spacing}$ = 340 and 370 nm, with $f \approx 0.32$ and 0.30, respectively. For the nanopillar grid with the largest $d_{spacing}$ of 410 nm, f was estimated to be 0.14, which is significantly smaller than that of the other two grids. Figure 3b displays R scaled by f, as a function of S. As observed from the figure, all three datasets collapse on the same curve upon scaling, indicating that the volume of available space within the grid is indeed the primary factor in determining the number of crystals that can nucleate and grow within the nanopillar grid.

Collectively, this analysis indicates that scaffold-directed crystallization of these crystals is a robust and reliable method for directing solution-phase crystal growth into 3D, interconnected arrays. By controlling the dip-coating speed and the dimensions of scaffold pillar structure, the ratio of (011)- to

https://dx.doi.org/10.1021/acsmaterialslett.0c00153
ACS Materials Lett. 2020, 2, 721–726

(100)-oriented crystals can be adjusted based on hydrodynamics and geometric principles. If the film height can be regulated not to exceed nanopillar heights during dip coating, it may be possible to completely suppress the formation of (100)-oriented crystals. Indeed, for samples in which S = 1.0 mm min^{-1} and $d_{spacing}$ = 410 nm, (100)-oriented crystals were rarely observed.

In conclusion, we demonstrate the use of graphoepitaxy to guide the crystallization of small-molecule organic semiconductor perylene into trellis structures consisting of single crystals. Our experiments suggest that this guided assembly is based on registry between periodicity of the underlying substrate relief structure and the crystal growth habit of perylene during Ostwald ripening at the air/solution/grid interface. The formation of interconnected, robust frameworks of small-molecule organic semiconductors opens new avenues to the assembly of complex device architectures for emerging optoelectronic applications. For devices requiring two organic semiconductors with large interfacial area to facilitate charge separation and recombination processes, such as organic solar cells and organic light-emitting diodes, for example, it follows that the theoretical ideal structure of active layers consists of interdigitated single-crystal domains of the two components. Furthermore, judicious design of the surface relief pattern introduced by the scaffolds and processing conditions will enable the assembly of organic semiconductor crystals in prespecified designs based on their crystal growth habit and desired properties. Critically, this method of graphoepitaxy-guided assembly results in the electrically active π-plane of the crystals exposed at the film surface, the optimal orientation of anisotropic organic semiconductors for solar cells, organic light-emitting diodes, and organic solid-state lasers. Beyond the field of organic electronics, high-surface energy planes typically possess enhanced materials properties, including reactivity and solubility, compared to low-surface-energy planes. Our strategy of graphoepitaxy-directed self-assembly may have broad implications across materials disciplines, from catalysts to pharmaceuticals.

■ ASSOCIATED CONTENT

Supporting Information

The Supporting Information is available free of charge at https://pubs.acs.org/doi/10.1021/acsmaterialslett.0c00153.

Experimental details and additional figures (PDF)

■ AUTHOR INFORMATION

Corresponding Author

Stephanie S. Lee − *Department of Chemical Engineering and Materials Science, Stevens Institute of Technology, Hoboken, New Jersey 07030, United States;* orcid.org/0000-0003-0964-6353; Email: stephanie.lee@stevens.edu

Authors

Kai Zong − *Department of Chemical Engineering and Materials Science, Stevens Institute of Technology, Hoboken, New Jersey 07030, United States*

Kaustubh M. Asawa − *Department of Mechanical Engineering, Stevens Institute of Technology, Hoboken, New Jersey 07030, United States*

Abigail Circelli − *Department of Chemical Engineering and Materials Science, Stevens Institute of Technology, Hoboken, New Jersey 07030, United States*

Nicholas Sparta − *Department of Chemical Engineering and Materials Science, Stevens Institute of Technology, Hoboken, New Jersey 07030, United States*

Chang-Hwan Choi − *Department of Mechanical Engineering, Stevens Institute of Technology, Hoboken, New Jersey 07030, United States;* orcid.org/0000-0003-2715-7393

Complete contact information is available at: https://pubs.acs.org/10.1021/acsmaterialslett.0c00153

Author Contributions

The manuscript was written through contributions of all authors. All authors have given approval to the final version of the manuscript.

Notes

The authors declare no competing financial interest.

■ ACKNOWLEDGMENTS

S.S.L. acknowledges support from the National Science Foundation, under Award No. CMMI-AM-1846178. The authors are also grateful for support from the PSEG Foundation to advance energy innovation at Stevens. C.-H.C. acknowledges support by the National Science Foundation, under Award No. CMMI-MME-1462499. The authors acknowledge the assistance of Dr. Chunhua Hu at the Department of Chemistry of New York University with 2D XRD experiments, and C.H. acknowledges support by the National Science Foundation, under Award No. CRIF/CHE-0840277 and by the NSF MRSEC Program, under Award No. DMR-0820341. Research used microscopy resources within the Laboratory for Multiscale Imaging at Stevens Institute of Technology and Dr. Tsengming Chou is acknowledged for his assistance. The authors thank Prof. M. D. Ward for helpful discussions. Research was performed in part at the Center for Functional Nanomaterials, Brookhaven National Laboratory, which is supported by the Department of Energy, Office of Basic Energy Sciences, under Contract No. DE-SC0012704.

■ REFERENCES

(1) Reese, C.; Bao, Z. Organic Single-Crystal Field-Effect Transistors. *Mater. Today* **2007**, *10*, 20−27.

(2) Gershenson, M. E.; Podzorov, V.; Morpurgo, A. F. Colloquium: Electronic Transport in Single-Crystal Organic Transistors. *Rev. Mod. Phys.* **2006**, *78*, 973−989.

(3) Lee, S. S.; Loo, Y.-L. Structural Complexities in the Active Layers of Organic Electronics. *Annu. Rev. Chem. Biomol. Eng.* **2010**, *1*, 59−78.

(4) Sundar, V. C.; Zaumseil, J.; Podzorov, V.; Menard, E.; Willett, R. L.; Someya, T.; Gershenson, M. E.; Rogers, J. A. Elastomeric Transistor Stamps: Reversible Probing of Charge Transport in Organic Crystals. *Science* **2004**, *303*, 1644−1646.

(5) Anthony, J. E.; Brooks, J. S.; Eaton, D. L.; Parkin, S. R. Functionalized Pentacene: Improved Electronic Properties from Control of Solid-State Order. *J. Am. Chem. Soc.* **2001**, *123*, 9482−9483.

(6) Zong, K.; Ma, Y.; Shayan, K.; Ly, J.; Renjilian, E.; Hu, C.; Strauf, S.; Briseño, A.; Lee, S. S. Directing Solution-Phase Nucleation to Form Organic Semiconductor Vertical Crystal Arrays. *Cryst. Growth Des.* **2019**, *19*, 3461−3468.

(7) Briseno, A. L.; Aizenberg, J.; Han, Y. J.; Penkala, R. A.; Moon, H.; Lovinger, A. J.; Kloc, C.; Bao, Z. Patterned Growth of Large Oriented Organic Semiconductor Single Crystals on Self-Assembled Monolayer Templates. *J. Am. Chem. Soc.* **2005**, *127*, 12164−12165.

(8) Geis, M. W.; Flanders, D. C.; Smith, H. I.; Antoniadis, D. A. Graphoepitaxy of Silicon on Fused Silica Using Surface Micropatterns and Laser Crystallization. *J. Vac. Sci. Technol.* **1979**, *16*, 1640−1643.

(9) Smith, H. I.; Geis, M. W.; Thompson, C. V.; Atwater, H. A. Silicon-on-Insulator by Graphoepitaxy and Zone-Melting Recrystallization of Patterned Films. *J. Cryst. Growth* **1983**, *63*, 527−546.
(10) Carter, P. W.; Ward, M. D. Topographically Directed Nucleation of Organic Crystals on Molecular Single-Crystal Substrates. *J. Am. Chem. Soc.* **1993**, *115*, 11521−11535.
(11) Bonafede, S. J.; Ward, M. D. Selective Nucleation and Growth of an Organic Polymorph by Ledge-Directed Epitaxy on a Molecular Crystal Substrate. *J. Am. Chem. Soc.* **1995**, *117*, 7853−7861.
(12) Diao, Y.; Harada, T.; Myerson, A. S.; Hatton, A. T.; Trout, B. L. The Role of Nanopore Shape in Surface-Induced Crystallization. *Nat. Mater.* **2011**, *10*, 867−871.
(13) Segalman, R. A.; Yokoyama, H.; Kramer, E. J. Graphoepitaxy of Spherical Domain Block Copolymer Films. *Adv. Mater.* **2001**, *13*, 1152−1155.
(14) Marencic, A. P.; Register, R. A. Controlling Order in Block Copolymer Thin Films for Nanopatterning Applications. *Annu. Rev. Chem. Biomol. Eng.* **2010**, *1*, 277−297.
(15) Bita, I.; Yang, J. K. W.; Jung, Y. S.; Ross, C. A.; Thomas, E. L.; Berggren, K. K. Graphoepitaxy of Self-Assembled Block Copolymers on Two-Dimensional Periodic Patterned Templates. *Science* **2008**, *321*, 939−943.
(16) Jo, P. S.; Vailionis, A.; Park, Y. M.; Salleo, A. Scalable Fabrication of Strongly Textured Organic Semiconductor Micropatterns by Capillary Force Lithography. *Adv. Mater.* **2012**, *24*, 3269−3274.
(17) Park, K. S.; Cho, B.; Baek, J.; Hwang, J. K.; Lee, H.; Sung, M. M. Single-Crystal Organic Nanowire Electronics by Direct Printing from Molecular Solutions. *Adv. Funct. Mater.* **2013**, *23*, 4758.
(18) Kong, X.; Zong, K.; Lee, S. S. Nanoconfining Optoelectronic Materials for Enhanced Performance and Stability. *Chem. Mater.* **2019**, *31*, 4953−4970.
(19) Ward, M. D.; Hunter, C. A.; Williams, N. H. Coordination Cages Based on Bis(Pyrazolylpyridine) Ligands: Structures, Dynamic Behavior, Guest Binding, and Catalysis. *Acc. Chem. Res.* **2018**, *51*, 2073−2082.
(20) Donaldson, D. M.; Robertson, J. M.; White, J. G. The Crystal and Molecular Structure of Perylene. *Proc. R. Soc. London. Ser. A. Math. Phys. Sci.* **1953**, *220*, 311−321.
(21) Tanaka, J. The Electronic Spectra of Aromatic Molecular Crystals. II. The Crystal Structure and Spectra of Perylene. *Bull. Chem. Soc. Jpn.* **1963**, *36*, 1237−1249.
(22) Rangel, T.; Rinn, A.; Sharifzadeh, S.; Da Jornada, F. H.; Pick, A.; Louie, S. G.; Witte, G.; Kronik, L.; Neaton, J. B.; Chatterjee, S. Low-Lying Excited States in Crystalline Perylene. *Proc. Natl. Acad. Sci. U. S. A.* **2018**, *115*, 284−289.
(23) Pick, A.; Klues, M.; Rinn, A.; Harms, K.; Chatterjee, S.; Witte, G. Polymorph-Selective Preparation and Structural Characterization of Perylene Single Crystals. *Cryst. Growth Des.* **2015**, *15*, 5495−5504.
(24) Fuke, K.; Kaya, K.; Kajiwara, T.; Nagakura, S. The Polarized Reflection and Absorption Spectra of Perylene Crystals in Monomeric and Dimeric Forms. *J. Mol. Spectrosc.* **1976**, *63*, 98−107.
(25) Diao, Y.; Tee, B. C.-K.; Giri, G.; Xu, J.; Kim, D. H.; Becerril, H. A.; Stoltenberg, R. M.; Lee, T. H.; Xue, G.; Mannsfeld, S. C. B.; Bao, Z. Solution Coating of Large-Area Organic Semiconductor Thin Films with Aligned Single-Crystalline Domains. *Nat. Mater.* **2013**, *12*, 665−671.
(26) Bai, X.; Zong, K.; Ly, J.; Mehta, J. S.; Hand, M.; Molnar, K.; Lee, S.; Kahr, B.; Mativetsky, J. M.; Briseno, A.; Lee, S. S. Orientation Control of Solution-Processed Organic Semiconductor Crystals to Improve Out-of-Plane Charge Mobility. *Chem. Mater.* **2017**, *29*, 7571−7578.
(27) Choi, C.-H.; Kim, C. J. Fabrication of a Dense Array of Tall Nanostructures over a Large Sample Area with Sidewall Profile and Tip Sharpness Control. *Nanotechnology* **2006**, *17*, 5326−5333.
(28) Wathuthanthri, I.; Mao, W.; Choi, C.-H. Two Degrees-of-Freedom Lloyd−Mirror Interferometer for Superior Pattern Coverage Area. *Opt. Lett.* **2011**, *36*, 1593−1595.
(29) Mao, W.; Wathuthanthri, I.; Choi, C.-H. Tunable Two-Mirror Interference Lithography System for Wafer-Scale Nanopatterning. *Opt. Lett.* **2011**, *36*, 3176−3178.
(30) El Mel, A. A.; Buffière, M.; Massuyeau, F.; Gautron, E.; Xu, W.; Choi, C.-H.; Wéry, J.; Faulques, E.; Barreau, N.; Tessier, P. Y. Direct Synthesis of ZnO Nanowires on Nanopatterned Surface by Magnetron Sputtering. *Chem. Vap. Deposition* **2011**, *17*, 337−341.
(31) Wathuthanthri, I.; Liu, Y.; Du, K.; Xu, W.; Choi, C.-H. Simple Holographic Patterning for High-Aspect-Ratio Three-Dimensional Nanostructures with Large Coverage Area. *Adv. Funct. Mater.* **2013**, *23*, 608−618.
(32) Bico, J.; Thiele, U.; Quéré, D. Wetting of Textured Surfaces. *Colloids Surf., A* **2002**, *206*, 41−46.
(33) Hamilton, B. D.; Ha, J.-M.; Hillmyer, M. A.; Ward, M. D. Manipulating Crystal Growth and Polymorphism by Confinement in Nanoscale Crystallization Chambers. *Acc. Chem. Res.* **2012**, *45*, 414−423.
(34) Jiang, Q.; Ward, M. D. Crystallization under Nanoscale Confinement. *Chem. Soc. Rev.* **2014**, *43*, 2066−2079.
(35) Davey, R. J.; Schroeder, S. L. M.; Ter Horst, J. H. Nucleation of Organic Crystals - A Molecular Perspective. *Angew. Chem., Int. Ed.* **2013**, *52*, 2166−2179.
(36) Le Berre, M.; Chen, Y.; Baigl, D. From Convective Assembly to Landau−Levich Deposition of Multilayered Phospholipid Films of Controlled Thickness. *Langmuir* **2009**, *25*, 2554−2557.
(37) Choi, C.-H.; Ulmanella, U.; Kim, J.; Ho, C. M.; Kim, C. J. Effective Slip and Friction Reduction in Nanograted Superhydrophobic Microchannels. *Phys. Fluids* **2006**, *18*, No. 087105.

https://dx.doi.org/10.1021/acsmaterialslett.0c00153
ACS Materials Lett. 2020, 2, 721−726